ChemPubSoc Europe

DOI: 10.1002/ejic.201901239

EurJIC European Journal of Inorganic Chemistry

Full Paper

Uranyl Borates

Two-Dimensional Uranyl Borates: From Conventional to Extreme Synthetic Conditions

Yucheng Hao,[a] Philip Kegler,[b] Thomas E. Albrecht-Schmitt,[c] Shuao Wang,[d] Qiang Dong,[a] and Evgeny V. Alekseev*[b]

Abstract: A systematic investigation of uranyl borates under different synthetic conditions resulted in five new 2D compounds, namely, $(H_3O)[(UO_2)(BO_3)]$, $Li[(UO_2)(BO_3)]\cdot(H_2O)$, α-$K_4[(UO_2)_5(BO_3)_2O_4]$, β-$K_4[(UO_2)_5(BO_3)_2O_4]$ and $K_{2.5}[(UO_2)_5(BO_3)_2O_{2.5}(OH)_{1.5}]\cdot(H_2O)_{2.5}$. $(H_3O)[(UO_2)(BO_3)]$ and $Li[(UO_2)(BO_3)]\cdot(H_2O)$ were obtained from hydrothermal reactions at 220 °C using the same mineralizer. Both materials possess the uranophane sheet topology with different symmetry of the unit cells. In the structure of $(H_3O)[(UO_2)(BO_3)]$ and $Li[(UO_2)(BO_3)]\cdot(H_2O)$, UO_7 pentagonal bipyramids share edges and vertexes with four BO_3 planar triangles. α-$K_4[(UO_2)_5(BO_3)_2O_4]$ and β-$K_4[(UO_2)_5(BO_3)_2O_4]$ are polytypes. α-$K_4[(UO_2)_5(BO_3)_2O_4]$ was synthesized from a high-temperature solid-state reaction under ambient pressure; whereas β-$K_4[(UO_2)_5(BO_3)_2O_4]$ was obtained from a high-temperature/high-pressure (HT/HP) reaction. Both structures have an identical anion topology, but β-$K_4[(UO_2)_5(BO_3)_2O_4]$ crystallizes in space group with higher symmetry. In $K_{2.5}[(UO_2)_5(BO_3)_2O_{2.5}(OH)_{1.5}]\cdot(H_2O)_{2.5}$, which was obtained from a hydrothermal reaction, UO_7 polyhedra share vertexes and edges with two independent BO_3 triangles, forming the most complex uranyl borate layers among all five compounds. The different synthetic routes, novel topologies, thermal behavior and Raman spectra are discussed.

1. Introduction

In the past two decades, uranium oxo-anion compounds have received considerable attention due to remarkable variety of their structures and interesting physicochemical properties.[1–3] As a result of these studies, the structural chemistry of uranium has been greatly expanded for both synthetic and natural materials.[1–4] One group of uranium bearing phases, oxo-anion based compounds such as carbonates, sulfates, silicates, phosphates and borates, etc, has been granted a special attention due to their important role in natural process of uranium migration.[5–9] Generally, the most common forms of uranium oxides are triuranium octoxide (U_3O_8) and the dioxide UO_2.[10] Both oxides are relatively stable over a wide range of environmental conditions.[10] Oxidation states of uranium ranges from +II to +VI in solid state phases,[11] and depending on the valence state, coordination chemistry of uranium varies dramatically.[2–10] However, it has to be noted that the oxidation states II, III and V are considerably less stable compared to tetravalent and hexavalent uranium.[2,11] Uranium in the hexavalent state usually forms linear or near-linear uranyl moieties, $(O=U=O)^{2+}$, with two short multiple U=O bonds ≈ 1.8 Å. Four or more oxygen atoms can be bound to the uranyl ion within the equatorial plane, configured into UO_6 tetragonal, UO_7 pentagonal, or UO_8 hexagonal bipyramids. A variety of connections between uranyl polyhedra exist creating unique structural diversity of uranium(VI) bearing materials.[3]

The oxo-borate materials, that may contain BO_3 triangles and/or BO_4 tetrahedra in countless connections, are remarkably complex due to the formation of zero-dimensional (0D) clusters, 1D chains, 2D sheets, and even zeolite-like 3D frameworks.[12–14] Usually, uranyl polyhedra (UO_6, UO_7 and UO_8) can connect in the equatorial plane BO_3 and/or BO_4 oxo-groups by vertex or edge sharing modes.[1–5] Uranyl borates represent a group of fascinating materials, because they possess rich and complex structural chemistry.[2]

Several synthetic methods have been adopted recently for the preparation of uranyl borates, such as slow evaporation from aqueous solutions, high-temperature solid-state reactions, hydrothermal-, and high temperature-high pressure (HT/HP) reactions. However, uranyl borates are difficult to synthesize in the presence of water because borates have weaker coordination affinity to uranyl ions in aqueous solutions.[1] Two uranyl

[a] School of Energy Materials and Chemical Engineering, Hefei University, Hefei 230000, China
[b] Institute of Energy and Climate Research (IEK-6), Forschungszentrum Jülich GmbH, 52428 Jülich, Germany
E-mail: e.alekseev@fz-juelich.de
https://www.fz-juelich.de
[c] Department of Chemistry and Biochemistry, Florida State University, 95 Chieftan Way, Tallahassee, FL 32306-4390, USA
[d] School for Radiological and Interdisciplinary Sciences (RAD-X) and Collaborative Innovation Center of Radiation Medicine of Jiangsu Higher Education Institutions, Jiangsu 215123, China

Supporting information and ORCID(s) from the author(s) for this article are available on the WWW under https://doi.org/10.1002/ejic.201901239.

borates, namely, $K_6[UO_2\{B_{16}O_{24}(OH)_8\}]\cdot(H_2O)_{12}$ and $Na_6[UO_2\{B_{16}O_{24}(OH)_8\}]\cdot(H_2O)_{14}$, were synthesized by slow evaporation methods.[15,16] A number of uranyl borate structures have been reported by Wang et al., being obtained using a H_3BO_3-flux method.[17–21] These compounds usually shared a common structural motif consisting of a linear uranyl core $(UO_2)^{2+}$ coordinated with polymerized network of BO_3 triangles and BO_4 tetrahedra.[1] A series of complex 2D potassium uranyl borates were prepared via a high-temperature/high-pressure (HT/HP) hydrothermal method (650 °C, 200 MPa) by Wu et al.[22] The first example of a mixed-valence U^{VI}/U^{V} borate, $K_{13}[(UO_2)_{19}(UO_4)(B_2O_5)_2(BO_3)_6(OH)_2O_5]\cdot H_2O$,[23] was obtained by Stritzinger et al. from a supercritical water reaction (600 °C, 200 MPa) with Ag-ampules playing the role of a soft reductant. The most striking feature in this structure is the tetra-oxo core unit, $[UO_4(OH)_2]$, that contains U^{V} with *trans* hydroxide anions. A pure U^{V} borate was recently synthesized and characterized using similar method with Ag ampules as soft reductant.[24] We can conclude here that structural motifs of uranyl borates are in strong correlation with the synthetic conditions and vary in a very wide range.

In this work we performed the synthesis and study of 2D uranyl borates from different synthetic conditions in order to demonstrate how changes in synthesis can give a rise to striking differences in structural properties. Herein, we report the syntheses of five novel uranyl borates; $(H_3O)[(UO_2)(BO_3)]$, $Li[(UO_2)(BO_3)]\cdot(H_2O)$, α-$K_4[(UO_2)_5(BO_3)_2O_4]$, β-$K_4[(UO_2)_5(BO_3)_2O_4]$, and $K_{2.5}[(UO_2)_5(BO_3)_2O_{2.5}(OH)_{1.5}]\cdot(H_2O)_{2.5}$ and discuss synthetic routes, structural topologies, thermal as well as spectroscopic properties of these phases.

2. Results and Discussion

2.1 Syntheses

Three different methods were applied in this work for the preparation of novel 2D uranyl borates. Among the five compounds, $(H_3O)[(UO_2)(BO_3)]$, $Li[(UO_2)(BO_3)]\cdot(H_2O)$ and $K_{2.5}[(UO_2)_5(BO_3)_2O_{2.5}(OH)_{1.5}]\cdot(H_2O)_{2.5}$ were prepared via hydrothermal synthetic method with different mineralizers, $Pb(NO_3)_2$ was used for $(H_3O)[(UO_2)(BO_3)]$ and $Li[(UO_2)(BO_3)]\cdot(H_2O)$, whereas $Zn(NO_3)_2$ is for $K_{2.5}[(UO_2)_5(BO_3)_2O_{2.5}(OH)_{1.5}]\cdot(H_2O)_{2.5}$. It is noted that, the boron sources for synthesis of $(H_3O)[(UO_2)(BO_3)]$, $Li[(UO_2)(BO_3)]\cdot(H_2O)$ and $K_{2.5}[(UO_2)_5(BO_3)_2O_{2.5}(OH)_{1.5}]\cdot(H_2O)_{2.5}$ are from the materials containing tetraborate $(B_4O_7)^{2-}$ anion, $Li_2B_4O_7$ for $(H_3O)[(UO_2)(BO_3)]$, $Li[(UO_2)(BO_3)]\cdot(H_2O)$ and $K_2B_4O_7$ for $K_{2.5}[(UO_2)_5(BO_3)_2O_{2.5}(OH)_{1.5}]\cdot(H_2O)_{2.5}$, respectively. Interestingly, despite the different reaction conditions all five compounds adopted 2D layered architectures. It is worth to compare these materials with uranyl borates obtained from melted H_3BO_3 flux. From the literature analysis, we found that most of the compounds prepared using H_3BO_3-flux have polymeric, infinite oxo-borate fragments in their structures.[1,2] Whereas, the phases that obtained in this work from hydrothermal method with tetraborates and large amount of water as a reaction medium are based on the isolated oxo-borate groups. Compound α-$K_4[(UO_2)_5(BO_3)_2O_4]$ was prepared by a typical high temperature solid state synthesis (980 °C) with excess of tetraborate as the reaction medium similar to that described for $Sr[(UO_2)_2(B_2O_5)O]$ synthesis.[9] However, in opposite to the 3D framework structure of $Sr[(UO_2)_2(B_2O_5)O]$,[9] α-$K_4[(UO_2)_5(BO_3)_2O_4]$ possesses a 2D layered structure. We presumed that a nature of counter cations plays a key role in the formation of these two compounds. The second polytype, β-$K_4[(UO_2)_5(BO_3)_2O_4]$ was obtained from a HT/HP (4GPa, 1000 °C) solid state reaction. Whereas, Wu et al. has prepared a chemically similar $K_4[(UO_2)_5(BO_3)_2O_4]\cdot H_2O$[23] from a different condition of (≈ 200 MPa, ≈ 650 °C).

2.2 Crystal Structures and Topologies of $(H_3O)[(UO_2)(BO_3)]$ and $Li[(UO_2)(BO_3)]\cdot(H_2O)$

$(H_3O)[(UO_2)(BO_3)]$ and $Li[(UO_2)(BO_3)]\cdot(H_2O)$ are stoichiometrically identical with the phases from $A(UO_2)(BO_3)$ (A = Li, Na, K, Rb, Cs) family reported previously, but structurally they are different.[31–33] $(H_3O)[(UO_2)(BO_3)]$ crystallizes in the centrosymmetric space group *Pbam*. There are two hydronium cations $(H_3O)^+$, two B, ten O and two U atoms in the asymmetric unit. $Li[(UO_2)(BO_3)]\cdot(H_2O)$ crystallizes in *Cmca* space group, with one Li, one B, one U and six O atoms in the asymmetric unit. Topologies of 2D layers in both structures are identical. This topology is well-known for inorganic uranium bearing materials and often called as uranophane anion topology.[34] The same topology has been observed in the structure of $K(UO_2)(BO_3)$.[33] The structure of both $(H_3O)[(UO_2)(BO_3)]$ and $Li[(UO_2)(BO_3)]\cdot(H_2O)$ is based on corrugated anionic uranyl borate layers, which are arranged in the *ab*-plane and H_3O^+ or Li^+ cations reside in the interlayer space (see Figure 1b, Figure 1c). Besides, water molecules are also presented in the interlayer space of $Li[(UO_2)(BO_3)]\cdot(H_2O)$. The presence of water molecules was confirmed by Raman spectroscopy (see Figure 8b). Accordingly, the interlayer distances in $Li[(UO_2)(BO_3)]\cdot(H_2O)$ are ≈ 7.73 Å and slightly larger than in $(H_3O)[(UO_2)(BO_3)]$, where such distances are ≈ 7.15 Å. Uranium atoms are seven-fold coordinated in both phases forming UO_7 pentagonal bipyramids, which are connected through edge sharing mode into 1D uranyl chains along the *a*-axis. The BO_3 triangles are corner or edge sharing linked to the uranyl chains, connecting them into the 2D uranyl borate layers parallel to the *ac*-plane (see Figure 1a, Figure 1e). The anion topology of $Li[(UO_2)(BO_3)]\cdot(H_2O)$is shown in Figure 1d ($UO_7$ polyhedra are shown in dark gray and BO_3 triangles are in green).[35] The axial U=O bond lengths in $(H_3O)[(UO_2)(BO_3)]$ are 1.74(3) Å and 1.80(3) Å, whereas the equatorial U–O bond lengths are in the range of [2.30(3)–2.47(2) Å]. The axial uranyl bonds in $Li[(UO_2)(BO_3)]\cdot(H_2O)$ are practically identical, 1.73(2) Å and 1.73(3) Å, and the equatorial U–O bond lengths are in the range of [2.28(1)–2.36(3) Å]. Bond valence sums (BVS) suggest that the U cation is 6+ in both structures. The B cation is 3+ based upon the BVS values of boron-oxygen. There is a number of hydrogen bonds between H_3O cations and oxygen atoms of the oxo-borate or uranyl groups, which provide connection between the uranyl borate layers. The Li^+ cations are four-fold coordinated in the structure of $Li[(UO_2)(BO_3)]\cdot(H_2O)$. They occupy the interlayer space and balancing the negative charge of

uranyl anionic layers. The Li–O bond lengths are in the range 1.92(8)–2.06(6) Å. The LiO_4 tetrahedra are vertex sharing along the a-axis, forming 1D Li–O chains, with Li–Li bond lengths of ca. 3.43 Å (see Figure S3). It is observed that the introduction of Li^+ cations results in the increase of the interlayer distance from $(H_3O)[(UO_2)(BO_3)]$ to $Li[(UO_2)(BO_3)]\cdot(H_2O)$, but without change of the uranyl borate layers topology.

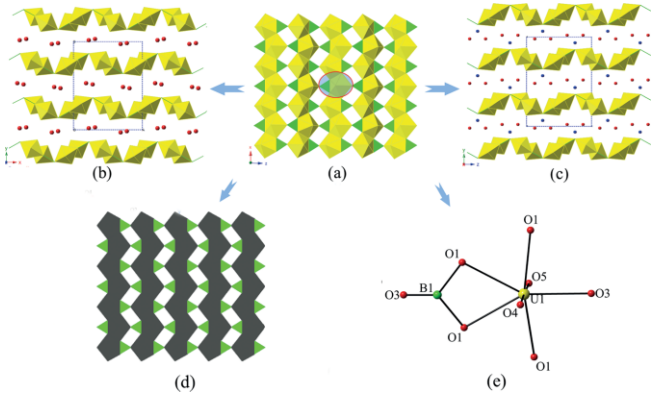

Figure 1. (a) A basic 2D uranyl borate sheet of compounds $(H_3O)[(UO_2)(BO_3)]$ and $Li[(UO_2)(BO_3)]\cdot(H_2O)$ (b) view of the structure $(H_3O)[(UO_2)(BO_3)]$ along the *c*-axis and (c) $Li[(UO_2)(BO_3)]\cdot(H_2O)$ along the *a*-axis, (d) anion topology observed of the uranyl borate sheet for $(H_3O)[(UO_2)(BO_3)]$ and $Li[(UO_2)(BO_3)]\cdot(H_2O)$, (e) a FBB $[(UO_2)(BO_3)]$ of the 2D UB sheet of $(H_3O)[(UO_2)(BO_3)]$and $Li[(UO_2)(BO_3)]\cdot(H_2O)$ with ball-and-stick mode. Uranyl polyhedra, $[(UO_2)O_5]$ pentagon in anion topology and BO_3 triangles are shown in yellow, gray and green, lithium and oxygen are shown in blue and red, respectively.

It is noteworthy that in the $A(UO_2)(BO_3)$ (A = H_3O, Li, Na, K, Rb, Cs) family,[31–33] H_3O, Li, Na and K-compounds have a common layered structural motif. However, Rb and Cs members have different and more complex topology, which implied that cations radii have played a key role for the structural architectures.[31–33] Noting that Li, Na and K-compounds possess the same sheet topology as $(H_3O)[(UO_2)(BO_3)]$ and $Li[(UO_2)(BO_3)]\cdot(H_2O)$, but the interlayer distances in $(H_3O)[(UO_2)(BO_3)]$ (ca. 7.3 Å) and $Li[(UO_2)(BO_3)]\cdot(H_2O)$ (ca. 7.7 Å) are significantly larger than that in anhydrous Li- (ca. 5.5 Å), Na- (ca. 5.7 Å) and K-phases (ca. 6.1 Å). It is presumed that with an increase of counter cations' radii, the interlayer distance increases in a direct proportion. However, H_3O^+ and H_2O made the layered distances larger than that observed in anhydrous Na- and K-phases. This trend can be explained by the radii of H_3O^+ and H_2O which are ≈ 2.0 Å and are significantly larger than that of Li^+ (≈ 0.8 Å), Na^+ (≈ 1.0 Å) and K^+ (≈ 1.4 Å).

Structural Features of α-$K_4[(UO_2)_5(BO_3)_2O_4]$ and β-$K_4[(UO_2)_5(BO_3)_2O_4]$

The compounds α-$K_4[(UO_2)_5(BO_3)_2O_4]$ and β-$K_4[(UO_2)_5(BO_3)_2O_4]$ have identical chemical compositions but crystallized in different space groups ($C2/_c$ and *Pbam*), thus these are polymorphic modifications. Both modifications possess layered structures with identical uranyl borate sheet topology. The layers are based upon three crystallographically independent uranium atoms and one boron atom. Two of the uranium atoms, U(1) and U(3) are seven-fold coordinated. The coordination environment can be described as a distorted pentagonal bipyramid. U(2) has an another coordination geometry displaying $U(2)O_6$ square bipyramid. $U(1)O_7$ and $U(3)O_7$ pentagonal bipyramids are connected alternately through sharing edges and vertex. One $U(2)O_4$ tetragonal bipyramid shares common vertex with $U(1)O_7$ and common edge with $U(3)O_7$, enclosed forming the U(1)–U(3)–U(1)–U(3)–U(2) 5-Membered Rings (MRs) in the 2D uranyl sheets within *bc*-plane. BO_3 triangles are edge sharing with $U(3)O_7$ and vertex sharing with $U(3)O_7$ in the structure of α-$K_4[(UO_2)_5(BO_3)_2O_4]$ as it is shown in Figure 2d. O(1), O(3), O(7), O(9) and O(10) are μ_3-oxygens shared by three uranyl groups or two uranyl units with a single BO_3 planar triangle (see Figure 2 and Figure 3).

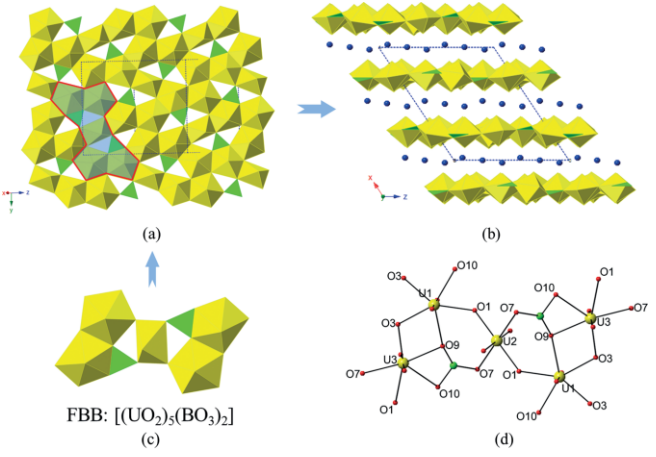

Figure 2. (a) A basic 2D uranyl borate sheet of compound α-$K_4[(UO_2)_5(BO_3)_2O_4]$on *bc*-plane, (b) view of the structure α-$K_4[(UO_2)_5(BO_3)_2O_4]$ along the *b*-axis, (c) a Fundamental Building Block (FBB) of the 2D UB sheet of α-$K_4[(UO_2)_5(BO_3)_2O_4]$ and the ball-and-stick mode (d). Uranyl polyhedra and BO_3 triangles are shown in yellow and green, potassium and oxygen are shown in blue and red, respectively.

For compound α-$K_4[(UO_2)_5(BO_3)_2O_4]$, the U=O axial bond lengths are ranging from 1.793(10) Å to 1.829(10) Å. The $U–O_{eq}$ bond lengths are ranging from 2.170(10) to 2.437(10) Å. The B–O bond lengths are in the range of[1.349(19) to 1.394(19) Å].

The BO_3 groups are nearly regular planar triangles with bond angles from 117.2(13)° to 121.2(13)°. The BVS results of U(1), U(2), U(3) and B(1) are closed to expected U^{6+} and B^{3+}. K^+ cations are resided in the interlayer space of both structures for balancing charges of the anionic layers. In β-$K_4[(UO_2)_5(BO_3)_2O_4]$, U–O distances for the axial uranyl bonds are in the range from 1.803(1) to 1.81(2) Å, whereas the equatorial $U–O_{eq}$ bond lengths of U–O ranges from 2.25(2) to 2.450(16) Å. The B–O bond lengths in BO_3 triangles are from 1.31(3) Å to 1.38(3) Å and the bond angles of O–B–O are in the range of 116(2)°–123(2)°. The BVS of U(1), U(2), U(3) and B(1) are closed to expected U^{6+} and B^{3+}.

In order to present the structure of uranyl borate layers more clearly, the Fundamental Building Blocks (FBB) of the 2D sheets together with the anion topology were provided on Figure 2c, Figure 2d, Figure 3c, Figure 3d and Figure 4. In the crystal-chemical classification of borate structures, FBB is the basic repeated clusters including BO_3/BO_4 compact or insular

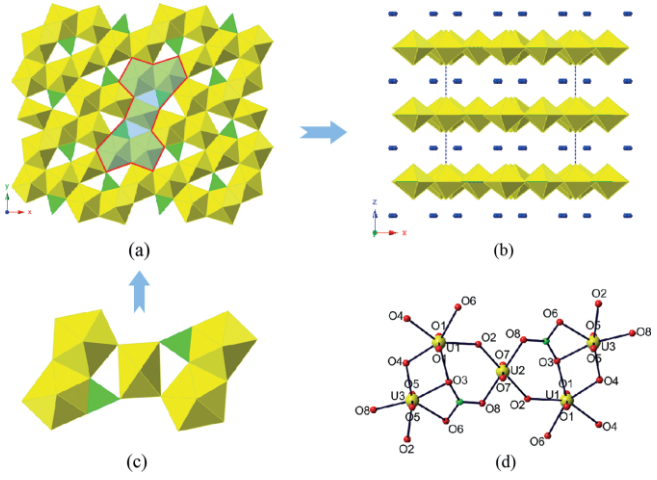

Figure 3. (a) A basic 2D uranyl borate sheet of compound β-$K_4[(UO_2)_5(BO_3)_2O_4]$on *ab*-plane, (b) view of the structure β-$K_4[(UO_2)_5(BO_3)_2O_4]$ along the *c*-axis, (c) a FBB of the 2D UB sheet of β-$K_4[(UO_2)_5(BO_3)_2O_4]$ and the ball-and-stick mode (d). Uranyl polyhedra and BO_3 triangles are shown in yellow and green, potassium and oxygen are shown in blue and red, respectively.

groups.[36] U(1)O_7 and U(3)O_7 polyhedra shared the edge to form a (U_2O_{12}) dimer. BO_3 triangle is further edge sharing with this U_2O_{12} dimer forming BU_2O_{13} uranyl borate group. Two BU_2O_{13} groups are centrosymmetric and further bridged by U(2)O_6 polyhedron finalizing the FBB of this layer (see Figure 2c, Figure 3c).

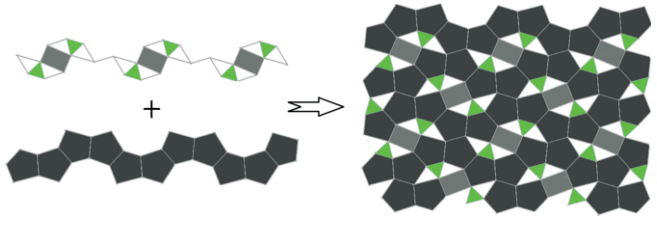

Figure 4. Anion topology observed in α-$K_4[(UO_2)_5(BO_3)_2O_4]$ and β-$K_4[(UO_2)_5(BO_3)_2O_4]$. U(2)O_2O_4 squares, U(1)O_2O_5, U(3)O_2O_5 pentagons and BO_3 triangles are shown in gray, dark gray and green, respectively.

It is worth to compare the structure of α-$K_4[(UO_2)_5(BO_3)_2O_4]$, β-$K_4[(UO_2)_5(BO_3)_2O_4]$ and their hydrated analogue $K_4[(UO_2)_5(BO_3)_2O_4](H_2O)$. These phases have identical uranyl borate layers, however, there are still some obvious differences between these phases, such as space groups, unit cell volumes and interlayer distances. The H_2O molecules in the interlayer space of $K_4[(UO_2)_5(BO_3)_2O_4](H_2O)$, cause larger interlayer distance and crystallization in a lower crystal symmetry than β-$K_4[(UO_2)_5(BO_3)_2O_4]$. α-$K_4[(UO_2)_5(BO_3)_2O_4]$ and β-$K_4[(UO_2)_5(BO_3)_2O_4]$ are polytypes because they have essentially identical chemical composition and topologies of the 2D sheets.[35] However, they have different symmetry and the stacking manner of layers. β-$K_4[(UO_2)_5(BO_3)_2O_4]$ crystallizes in orthorhombic *Pbam* group, whereas α-$K_4[(UO_2)_5(BO_3)_2O_4]$ crystallizes in monoclinic *C*2/*c* space group. It is forwarded by different arrangement of 2D layers in both structures. The 2D layers in α-$K_4[(UO_2)_5(BO_3)_2O_4]$ have a 0.5*c* shift one over another within *bc*-plane. However, layers in β-$K_4[(UO_2)_5(BO_3)_2O_4]$, demonstrate no shift within *ab*-plane (analog of *bc*-plane in alpha phase). The stacking modes of the layers in both polytypes are also different. For α-$K_4[(UO_2)_5(BO_3)_2O_4]$, the uranyl borate layers are stacking as ...*ABABAB*... Whereas the uranyl borate layers stacking mode in β-$K_4[(UO_2)_5(BO_3)_2O_4]$ is in an order of ...*AA-AAAA*... The interlayer distances of both polytypes are quite similar ≈ 6.8 Å.

Structure of $K_{2.5}[(UO_2)_5(BO_3)_2O_{2.5}(OH)_{1.5}]\cdot(H_2O)_{2.5}$

Compound $K_{2.5}[(UO_2)_5(BO_3)_2O_{2.5}(OH)_{1.5}]\cdot(H_2O)_{2.5}$ crystallizes in the orthorhombic space group *Pbam* and possesses a more complex structural topology than the four materials discussed above. It contains five unique U^{6+} sites U(1)–U(5) and two independent boron atoms B(1) and B(2) in the asymmetric unit. It has to be noted that the compounds α-$K_4[(UO_2)_5(BO_3)_2O_4]$, β-$K_4[(UO_2)_5(BO_3)_2O_4]$ and $K_{2.5}[(UO_2)_5(BO_3)_2O_{2.5}(OH)_{1.5}]\cdot(H_2O)_{2.5}$ have the same U/B molar ratio 5:2. However, the 2D layers in $K_{2.5}[(UO_2)_5(BO_3)_2O_{2.5}(OH)_{1.5}]\cdot(H_2O)_{2.5}$ is different compared to α-$K_4[(UO_2)_5(BO_3)_2O_4]$ and β-$K_4[(UO_2)_5(BO_3)_2O_4]$. All uranium sites in $K_{2.5}[(UO_2)_5(BO_3)_2O_{2.5}(OH)_{1.5}]\cdot(H_2O)_{2.5}$ are existing as UO_7 pentagonal bipyramids. Both boron atoms (B1 and B2) adopted planar three-fold oxygen coordination. FBB of these layers are stoichiometrically identical to α-$K_4[(UO_2)_5(BO_3)_2O_4]$ and β-$K_4[(UO_2)_5(BO_3)_2O_4]$(see Figure 5a, Figure 5c). U(1) and U(5) share the common edge O(2)–O(12) created a U_2O_{12}dimer. The B(1)O_3triangle linked with the dimer U(1)–U(5) to form a uranyl borate group of$[B(UO_2)_2]$. The U(4)O_7 pentagonal bipyramids are further connected with two centrosymmetric $[B(UO_2)_2]$ groups to form the FBB via corner- and edge-sharing. O(2) are μ_4-oxygens shared by three uranyl groups and planar BO_3 triangles, which can be observed in $K_{15}[(UO_2)_{18}(BO_3)_7O_{15}]$[15] (see Figure 5d). However, O(8), O(9), O(10), O(11), O(12), O(14) and O(15) are μ_3-oxygens shared by three uranyl groups or two uranyl groups with one BO_3 triangle.

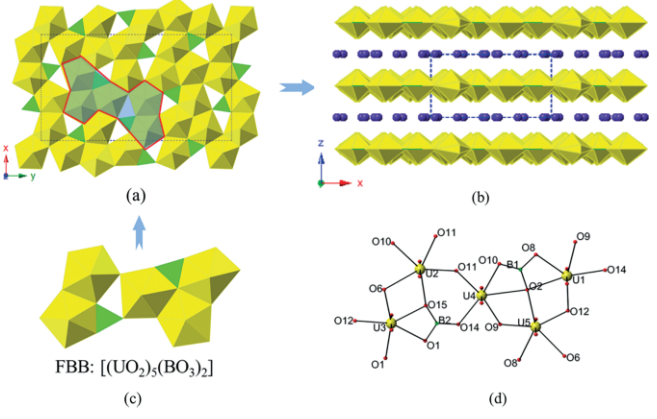

Figure 5. (a) A 2D uranyl borate sheet of compound $K_{2.5}[(UO_2)_5(BO_3)_2O_{2.5}(OH)_{1.5}]\cdot(H_2O)_{2.5}$on *ab*-plane, (b) view of the structure $K_{2.5}[(UO_2)_5(BO_3)_2O_{2.5}(OH)_{1.5}]\cdot(H_2O)_{2.5}$ along the *a*-axis, (c) the FBB of the 2D UB sheet of $K_{2.5}[(UO_2)_5(BO_3)_2O_{2.5}(OH)_{1.5}]\cdot(H_2O)_{2.5}$ and (d) the ball-and-stick fashion.

The axial U=O bond lengths for the uranyl cations are from 1.759(18) Å to 1.790(14) Å. The bond lengths of U–O_{eq} are in the range of [2.189(16)-2.861(14) Å]. The B–O bond lengths are

ranging from 1.34(3) to 1.38(3) Å, and the O–B–O bond angles are ranging from 116(2)° to 124(2)°. The BVS for B(1), B(2), U(1)–U(5) and K(1), K(2), K(3) atoms suggest that B, U and K atoms are in oxidation states of +3, +6 and +1,respectively. The BVS values for O(1) to O(15) are 2.17, 1.97, 2.03, 1.97, 1.99, 1.19, 1.76, 2.07, 2.12, 2.14, 1.93, 2.01, 1.91, 2.11 and 2.07, respectively. Based upon the BVS, the local coordination environment of oxygen atoms and with the charge balance of the whole structure, we conclude that O(6) atoms are fully occupied hydroxyl (OH^-) groups. Speculatively, O(7) is as partially occupied $(OH^-)_{0.5}$ position and all other oxygen atoms are O^{2-}.

The 2D layers in $K_{2.5}[(UO_2)_5(BO_3)_2O_{2.5}(OH)_{1.5}]\cdot(H_2O)_{2.5}$ is based upon 5-Uranium Membered Rings (5U-MRs), which are similar to that in α-$K_4[(UO_2)_5(BO_3)_2O_4]$ and β-$K_4[(UO_2)_5(BO_3)_2O_4]$. The distances between the uranyl borate layers are ca. 6.98 Å and are larger than that in α-$K_4[(UO_2)_5(BO_3)_2O_4]$ and β-$K_4[(UO_2)_5(BO_3)_2O_4]$. K^+ cations are located between the layers as well as the water molecules (see Figure 5b). The K^+ cations are six or seven-fold coordinated with K–O bond lengths from 2.776(14) to 2.986(1) Å. The existence of disordered water molecules makes the distance between the layers larger than that in the structure of α-$K_4[(UO_2)_5(BO_3)_2O_4]$ and β-$K_4[(UO_2)_5(BO_3)_2O_4]$. In order to describe the topology of layers in $K_{2.5}[(UO_2)_5(BO_3)_2O_{2.5}(OH)_{1.5}]\cdot(H_2O)_{2.5}$, we simplified the anionic layers of $K_{2.5}[(UO_2)_5(BO_3)_2O_{2.5}(OH)_{1.5}]\cdot(H_2O)_{2.5}$ by omitting the oxygen anions and kept the connectivity between the B and U cations. The simplified U–B net was observed as a new 7-nodal net topological type with a point symbol[37–39] of $\{3^5.4^5\}_2\{3^6.4^6.5^3\}_3\{3^7.4^7.5^7\}_2$ (see Figure S5). The topology of the 2D sheets can also be depicted using the anion topology method.[35] The 2D anion sheets of $K_{2.5}[(UO_2)_5(BO_3)_2O_{2.5}(OH)_{1.5}]\cdot(H_2O)_{2.5}$ are constructed by pseudo *P* chains proposed by Burns.[35] Here one pentagon links to two other pentagons, denoted as P_s chains and are shown in dark gray. *P* chains are shown in gray and to be bridged with modified *R* chains. The *R* chains are based on two isolated BO_3 triangles, and denoted as R_b chains which are shown in green in Figure 6. This shows that compound $K_{2.5}[(UO_2)_5(BO_3)_2O_{2.5}(OH)_{1.5}]\cdot(H_2O)_{2.5}$ has a complex distorted sayrite $Pb_2(UO_2)_5O_6(OH)_2\cdot(H_2O)_4$ topology compared to that in α-$K_4[(UO_2)_5(BO_3)_2O_4]$ and β-$K_4[(UO_2)_5(BO_3)_2O_4]$. This anion topology is built on *P* chains, alternating pentagon units in the P_s chains where the positions of squares within the *R* chains are substituted by two sorts of BO_3 triangles with the following sequence ...$PR_bP_sPR_bP_sPR_bP_s$...[40]

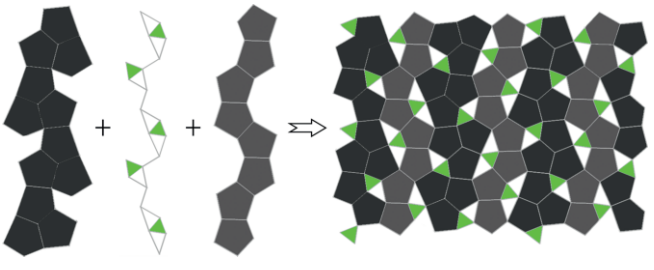

Figure 6. Anion topology observed in $K_{2.5}[(UO_2)_5(BO_3)_2O_{2.5}(OH)_{1.5}]\cdot(H_2O)_{2.5}$. $U(2)O_2O_5$, $U(3)O_2O_5$ pentagons, $U(1)O_2O_5$, $U(4)O_2O_5$ $U(5)O_2O_5$ pentagons and BO_3 triangles are shown in gray, dark gray and green, respectively.

2.3 Local Configurations of Boron and Uranium Centers

The structural variety of uranyl borates arise from the diversity of uranium coordination chemistry and tendency of oxo-borates polymeriszation.[1–3] Boron atoms form planar BO_3 triangles in all five compounds. The uranium atoms are existing as UO_6 tetragonal and UO_7 pentagonal bipyramids. For $(H_3O)[(UO_2)(BO_3)]$ and $Li[(UO_2)(BO_3)]\cdot(H_2O)$, the geometrical environments of borate anions is BU_4, in which one BO_3 planar triangle linked with three UO_7 pentagonal bipyramids via vertex sharing and one by edge sharing (see Figure 7a). In α-$K_4[(UO_2)_5(BO_3)_2O_4]$, β-$K_4[(UO_2)_5(BO_3)_2O_4]$ and $K_{2.5}[(UO_2)_5(BO_3)_2O_{2.5}(OH)_{1.5}]\cdot(H_2O)_{2.5}$, all the BO_3 anion groups are coordinated with five uranyl polyhedra, forming BU_5 pentagons. In α-$K_4[(UO_2)_5(BO_3)_2O_4]$ and β-$K_4[(UO_2)_5(BO_3)_2O_4]$ borate anions are linked with four UO_7 and one UO_6 polyhedra via sharing edges and corners (see Figure 7b). In $K_{2.5}[(UO_2)_5(BO_3)_2O_{2.5}(OH)_{1.5}]\cdot(H_2O)_{2.5}$ planar BO_3 triangles are edge sharing with two and corner sharing with three UO_7 pentagonal bipyramids (see Figure 7b and Figure 7c). The connection mode BU_5 in $K_{2.5}[(UO_2)_5(BO_3)_2O_{2.5}(OH)_{1.5}]\cdot(H_2O)_{2.5}$ was uncovered for the first time in the 2D uranyl borates family[1–3] (see Figure 7c). Both UO_6 tetragonal and UO_7 pentagonal bipyramids were observed in the structures of reported compounds. Five different geometries of local environment of uranium centers were found in the studied five structures (see Figure 7d–h). The first one is built upon five components, which are UO_7 pentagonal bipyramid and four planar oxo-borate triangles. This geometry is existing in the structures of $(H_3O)[(UO_2)(BO_3)]$, $Li[(UO_2)(BO_3)]\cdot(H_2O)$ and also spread within the series of $A(UO_2)(BO_3)$ (*A* = Li, Na, K)[31–33] (see Figure 7f). The uranium center geometries presented on Figure 7e, 7f and 7g has been observed in the structures of α-$K_4[(UO_2)_5(BO_3)_2O_4]$ and β-$K_4[(UO_2)_5(BO_3)_2O_4]$. These geometries are resemble to that existing in the structure of $K_4[(UO_2)_5(BO_3)_2O_4](H_2O)$.[23]

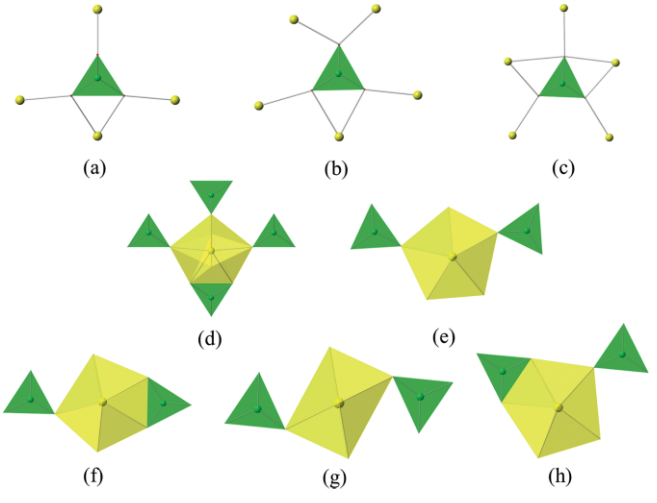

Figure 7. Local geometrical configurations of boron or uranium center in all five compounds. (a)–(c) are the coordination environments of BO_3 triangles, (d)–[h] are the coordination chemistry of uranyl polyhedra. (a), (d) are in $(H_3O)[(UO_2)(BO_3)]$ and $Li[(UO_2)(BO_3)]\cdot(H_2O)$; (b), (e), (f) and (g) in α-$K_4[(UO_2)_5(BO_3)_2O_4]$and β-$K_4[(UO_2)_5(BO_3)_2O_4]$; (b), (c), (e), (f) and [h] are from $K_{2.5}[(UO_2)_5(BO_3)_2O_{2.5}(OH)_{1.5}]\cdot(H_2O)_{2.5}$.

2.4 Comparison of the Different U/B Ratios and the FBBs in the Uranyl Borates Family

Analysis of the literature data reveals that more than 30 uranyl borates have been reported to date. The structural features of these phases are strongly dependent on counter cation nature. Moreover, the structural chemistry of uranyl borates has a correlation to the U/B (uranium to boron) molar ratio. The uranyl borates with different U/B molar ratios and corresponding uranyl borate clusters are presented in Table S2.

To compare the differences of the uranyl borate structures, we have separated them into two parts. In the first one the U/B molar ratio is less than 1 and in the second part it is larger than 1 (see Table S1). The simplest series of uranyl borates is $A(UO_2)(BO_3)$ (A =H_3O, Li, Na, K, Rb, Cs)[31–33] with U/B ratio = 1. These phases possess the same FBB of $[(UO_2)(BO_3)]^-$. The FBBs are linked with each other forming the infinite 2D uranyl borate layers. The 2D layers of $A(UO_2)(BO_3)$ (A = Li, Na, K)[31–33] are have a well-known uranophane anion topology,[34] however, the layers in Rb and Cs members of the series exhibit a highly distorted uranophane topology. This implies that the counter cation radius has an impact on the structural topologies in this series. The U/B ratio of $Mg[(UO_2)B_2O_5]$[32] is 1:2 with $[(UO_2)(B_2O_5)]^{2-}$ FBB. $[(UO_2)(B_2O_5)]^{2-}$ is based upon one UO_7 pentagonal bipyramid edge shared with a B_2O_5 dimer and form the infinite 2D sheets in the structure of $Mg[(UO_2)B_2O_5]$.[32] $Ni_7[(UO_2)(BO_4)_2](BO_3)_2$ exhibits a U/B molar ratio of 1:4 in the asymmetric unit.[41] However, $Ni_7[(UO_2)(BO_4)_2](BO_3)_2$ is a chain structure with $[(UO_2)(BO_4)_2]^{8-}$ FBB and the planar BO_3 triangles are isolated between uranyl borate chains. Compounds $Li[(UO_2)B_5O_9]\cdot 3H_2O$,[20] $Na[(UO_2)_2B_{10}O_{15}(OH)_5]$,[42] $K[(UO_2)_2B_{10}O_{15}(OH)_5]$, $Rb[(UO_2)_2B_{10}O_{16}(OH)_3]\cdot 0.7H_2O$,[18] $Tl[(UO_2)_2B_{10}O_{16}(OH)_3]$[42] and $Ag[(UO_2)B_5O_8(OH)_2]$[20] possess the same U/B molar ratios as 1:5. All the FBBs of them can be described as $[(UO_2)B_5O_9]^-$. The U/B ratios of $Na[(UO_2)B_6O_{10}(OH)]\cdot 2H_2O$,[42] $K_2[(UO_2)_2B_{12}O_{19}(OH)_4]\cdot 0.3H_2O$[18] and $K[(UO_2)(B_6O_{10}OH)]$[43] are 1:6 with the FBB as $[(UO_2)B_6O_{11}]^{2-}$. The compounds with U/B molar ratios of ≈ 1:5 and ≈ 1:6 share a common structural motif. In this motif, one UO_8 polyhedra is surrounded by nine polymerized borate units which is based on the variative connections of BO_3 triangles and BO_4 tetrahedra. The lowest U/B ratio is 1:16 and was observed in $Na_6[UO_2\{B_{16}O_{24}(OH)_8\}]\cdot(H_2O)_{14}$[17] and $K_6[UO_2\{B_{16}O_{24}(OH)_8\}]\cdot(H_2O)_{12}$.[16] The structures of them are based on 0D nano-size cluster with complex $[(UO_2)(B_{16}O_{32})]^{14-}$ anion encapsulating uranyl groups. Here we can see that with increasing of boron content, the structure dimensionality increases and reaches its 3D maximum at U/B ≈ 1:7 ratio and then dropping down with forming of 0D clusters at extreme low U to B ratios.

Another group of uranyl borates with totally different structural arrangement is a series of phases with U/B molar ratios more than 1. The U/B molar ratios of $K_4[(UO_2)_5(BO_3)_2O_4]\cdot H_2O$[23] and $M[(UO_2)_5(BO_3)_2O_2(OH)_2]\cdot(H_2O)_5$ (M = Sr, Ba)[9] are 5:2 with the FBB $[(UO_2)_5(BO_3)_2O_4]^{4-}$. A relatively high U/B ratio (13:6) observed in the first mixed alkali and alkali-earth metal uranyl borates $K_4Sr_4[(UO_2)_{13}(B_2O_5)_2(BO_3)_2O_{12}]$.[44] Its FBB is $[(UO_2)_{13}(B_2O_5)_2(BO_3)_2O_{12}]^{12-}$, which is built from the connections of three UO_8, ten UO_7 polyhedra, two B_2O_5 dimers and two BO_3 triangles. The highest U/B ratio 18:7 has been observed in $K_{15}[(UO_2)_{18}(BO_3)_7O_{15}]$[23] with a FBB of $[(UO_2)_{18}(BO_3)_7O_{15}]^{15-}$. One UO_8, one UO_6 and sixteen UO_7 polyhedra and seven BO_3 triangles connected via corner or edge sharing constructed into the FBB $[(UO_2)_{18}(BO_3)_7O_{15}]^{15-}$. It is apparently to see that, with the increasing of U-content in the FBB, the anion topologies of the 2D layers become more complex – from $[(UO_2)(BO_3)]^-$ to $[(UO_2)_{18}(BO_3)_7O_{15}]_n^{15-}$. Most of the phases with complex topologies and rich uranium content have been obtained from hydrothermal and solid state reactions under extreme pressure. Hence, we supposed that the most complex structures usually come from chemical systems where oxo-boron fragments are not tend to polymerize. The structures of these materials are more like uranium oxides while materials with high boron content are structurally closer to oxo-salts.

2.5 Thermal Analyses and Raman Spectroscopy

The differential scanning calorimetry (DSC) analysis coupled with thermogravimetry (TG) curves in the temperature range from 50 to 1200 °C for α-$K_4[(UO_2)_5(BO_3)_2O_4]$ and $K_{2.5}[(UO_2)_5(BO_3)_2O_{2.5}(OH)_{1.5}]\cdot(H_2O)_{2.5}$ polycrystalline phases are shown in Figure 8. There is no obvious weight loss based on the TG curve of α-$K_4[(UO_2)_5(BO_3)_2O_4]$. The DSC curve shows a strong endothermic peak at around 943 °C, which corresponds to the melting of the compound (see Figure 8a). For

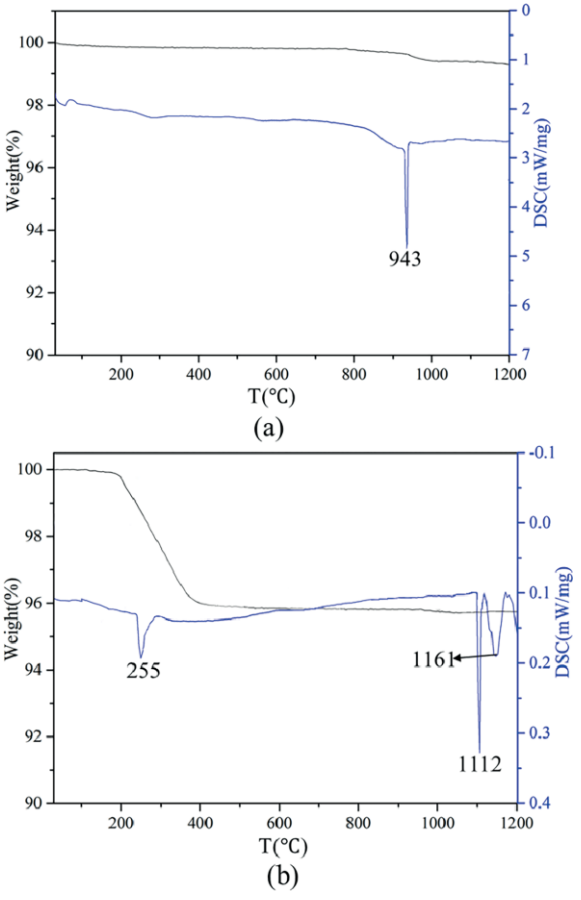

Figure 8. TG-DSC curves of α-$K_4[(UO_2)_5(BO_3)_2O_4]$ and $K_{2.5}[(UO_2)_5(BO_3)_2O_{2.5}(OH)_{1.5}]\cdot(H_2O)_{2.5}$.

$K_{2.5}[(UO_2)_5(BO_3)_2O_{2.5}(OH)_{1.5}]\cdot(H_2O)_{2.5}$,TG analysis shows a weight loss around 200 °C, which corresponds to the loss of 3 water molecules per formula unit. The mass loss of 4.05 % observed from the TG curve is in good agreement with the calculated one (3.51 %). An endothermic peak on the DSC-curve at 255 °C supports our assumption. The endothermic peak at 1112 °C and 1161 °C correspond to the melting and decomposition of the dehydrated product (Figure 8b).

The Raman spectra of $(H_3O)[(UO_2)(BO_3)]$, $Li[(UO_2)(BO_3)]\cdot(H_2O)$ and $K_{2.5}[(UO_2)_5(BO_3)_2O_{2.5}(OH)_{1.5}]\cdot(H_2O)_{2.5}$ were measured in the range of 100–4000 cm^{-1} and for α-$K_4[(UO_2)_5(BO_3)_2O_4]$ and β-$K_4[(UO_2)_5(BO_3)_2O_4]$ in the range of 100–1600 cm^{-1}. It is obvious that modes at the low frequency part between 100 and 300 cm^{-1} are contributed from the vibrations of the "lattice skeleton". The Raman spectra of $(H_3O)[(UO_2)(BO_3)]$ and $Li[(UO_2)(BO_3)]\cdot(H_2O)$, shown in Figure 9a and Figure 9b, are reflecting the isotypic structure relationship of these phases. Only a small difference between spectra can be observed. There are more scattering peaks with stronger intensity in the section (100–1600cm^{-1}), which is dominated by the vibration modes of the uranium polyhedra.

For these two compounds, the Raman spectra show strong and sharp bands around 800 cm^{-1} due to the symmetric vibration υ_1 mode of the uranyl ion with short uranyl U–O bond lengths of around 1.80Å.[16] Raman bands with very weak peaks around 1293 and 971 cm^{-1} have been assigned to the asymmetric and symmetric stretching υ_1, υ_3 modes of the B–O bonds in BO_3. The vibration modes from H_3O^+ cation with weak peaks are observed at around 2950 and 3054 cm^{-1}, whereas the peaks around 3540 cm^{-1} are originating from the vibration of coordinated water molecules in $Li[(UO_2)(BO_3)]\cdot(H_2O)$.

The Raman spectra of isotypical layered structures of α-$K_4[(UO_2)_5(BO_3)_2O_4]$ and β-$K_4[(UO_2)_5(BO_3)_2O_4]$ are shown in Figure 9c,d. The peaks from the range 730–860 cm^{-1} could be assigned to the symmetric stretching υ_1 mode of the uranyl groups in both compounds. The Raman bands within 980–1200 cm^{-1} can be attributed to the asymmetric and symmetric stretching modes of the B–O bonds in BO_3 triangles. The doubly degenerated in-plane O–B–O bending mode is observed at around 530–700 cm^{-1} and the doubly degenerated asymmetrical stretching mode is observed in the range from 1250 to 1500 cm^{-1}.[44–48] The Raman spectrum of $K_{2.5}[(UO_2)_5(BO_3)_2$-

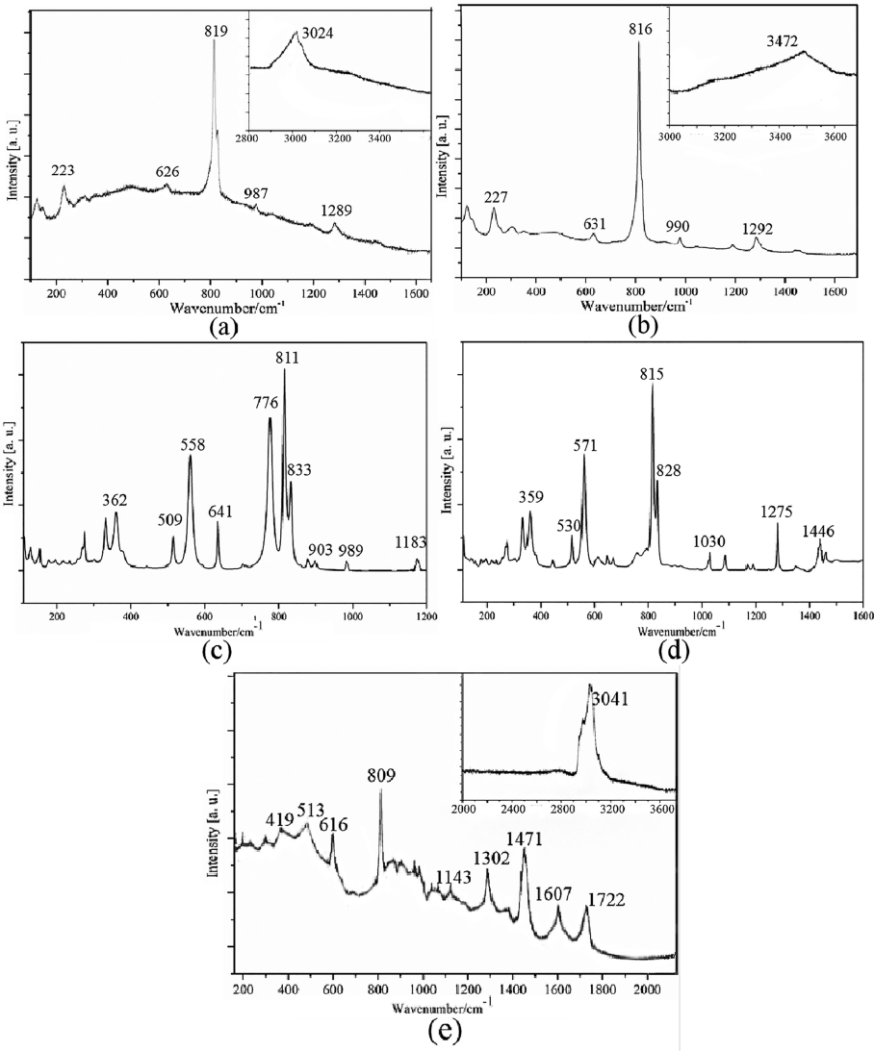

Figure 9. Raman shifts of $(H_3O)[(UO_2)(BO_3)]$(a),$Li[(UO_2)(BO_3)]\cdot(H_2O)$ (b), α-$K_4[(UO_2)_5(BO_3)_2O_4]$ (c),β-$K_4[(UO_2)_5(BO_3)_2O_4]$(d) and $K_{2.5}[(UO_2)_5(BO_3)_2O_{2.5}$-$(OH)_{1.5}]\cdot(H_2O)_{2.5}$ (e).

$O_{2.5}(OH)_{1.5}]\cdot(H_2O)_{2.5}$ shows a strong and sharp peak at 836 cm^{-1} which can be assigned to the symmetric vibration υ_1 mode of the uranyl group. The Raman bands in the range of 480–680 cm^{-1} are attributed to the doubly degenerated O–B–O bending mode in BO_3 triangles. The weak peaks between 900 and 1150 cm^{-1} are caused from the symmetrical stretching mode of BO_3 units. The strong Raman bands in the range of 1270–1500 cm^{-1} can be assigned to the doubly degenerated asymmetrical stretching mode of BO_3 groups. The vibrational modes of coordinated water molecules are located at the bands of 1600 –1800cm^{-1} and 3040cm^{-1} (see Figure 9e). These assignments are consistent with the previously reported works.[9,43,47]

3. Conclusions

A series of uranyl borates, namely, $(H_3O)[(UO_2)(BO_3)]$, $Li[(UO_2)(BO_3)]\cdot(H_2O)$, α-$K_4[(UO_2)_5(BO_3)_2O_4]$, β-$K_4[(UO_2)_5(BO_3)_2O_4]$ and $K_{2.5}[(UO_2)_5(BO_3)_2O_{2.5}(OH)_{1.5}]\cdot(H_2O)_{2.5}$ have been obtained from different conditions and well characterized. In this study, we have adopted three different methodologies for preparation of the novel uranyl borate phases. This study demonstrates that layered uranyl borates can form in a wide range of conditions. The chemical composition of the flux, the amount of water in reaction media, the nature of counter cations and physical conditions are the key factors for the formation of uranyl borates.

$(H_3O)[(UO_2)(BO_3)]$ and $Li[(UO_2)(BO_3)]\cdot(H_2O)$ are stoichiometrically identical and comprise 2D $[(UO_2)(BO_3)]^-$ units isolated by hydronium or lithium cations. It is interesting to note that a slightly change of the initial reagents and the constant use of the same mineralizer, leads to no change of the structural topology from $(H_3O)[(UO_2)(BO_3)]$ to $(H_3O)[(UO_2)(BO_3)]$. However, changing the mineralizer from $Pb(NO_3)_2$ to $Zn(NO_3)_2$, give rise to the most complex 2D layered structure $[(UO_2)_5(BO_3)_2O_4]^{2-}$ of $K_{2.5}[(UO_2)_5(BO_3)_2O_{2.5}(OH)_{1.5}]\cdot(H_2O)_{2.5}$ among the five uranyl borates, due to the various local geometrical configurations of uranyl cations. This fact demonstrates that the mineralizer together with physical parameters of synthetic conditions play a key role in structural formation of uranyl borates. Two polymorphs of {α-$K_4[(UO_2)_5(BO_3)_2O_4]$ and β-$K_4[(UO_2)_5(BO_3)_2O_4]$} compared to $K_{2.5}[(UO_2)_5(BO_3)_2O_{2.5}(OH)_{1.5}]\cdot(H_2O)_{2.5}$ have shown the structural flexibility of the layered potassium uranyl borates. α-$K_4[(UO_2)_5(BO_3)_2O_4]$ and β-$K_4[(UO_2)_5(BO_3)_2O_4]$ possess the identical[$(UO_2)_5(BO_3)_2O_4]^{4-}$ uranyl borate layers of, but β-$K_4[(UO_2)_5(BO_3)_2O_4]$ crystallizes in higher symmetry than α-$K_4[(UO_2)_5(BO_3)_2O_4]$. Speculatively, pressure may stabilize the beta phase which could not be thermodynamically stable at normal conditions. The relations between different U/B ratios and the structural complexity of the uranyl borates have been reviewed in this work. We have demonstrated that the complexity of structural topology significantly increases with an increase of U/B ratio deviation from **1**.

4. Experimental Section

Caution! The $UO_2(NO_3)_2\cdot(H_2O)_6$ used in this study contains natural uranium, nevertheless the standard precautions for handling radioactive materials must be followed.

4.1 Materials and Methods: Uranyl nitrate $UO_2(NO_3)_2\cdot(H_2O)_6$(International Bioanalytical Industries, Inc.), lead nitrate $Pb(NO_3)_2$(Alfa-Aesar, 99.9 %), potassium nitrate KNO_3 (Alfa-Aesar, 99.9 %), lithium tetraborate $Li_2B_4O_7$ (Alfa-Aesar, 99.9 %), potassium tetraborate $K_2B_4O_7\cdot(H_2O)_4$ (Alfa-Aesar, 99.9 %), and boric acid H_3BO_3 (Alfa-Aesar, 97 %) were all used as received.

4.1.1 Syntheses of $(H_3O)[(UO_2)(BO_3)]$ and $Li[(UO_2)(BO_3)]\cdot(H_2O)$: Both compounds were prepared by a hydrothermal method. The mixtures of $UO_2(NO_3)_2\cdot(H_2O)_6$ (0.0516 g, 0.10 mmol), $Pb(NO_3)_2$ (0.0332 g, 0.10 mmol), $Li_2B_4O_7$(0.0426 g, 0.25 mmol) and deionized water (0.5 mL), in a ratio of U/Pb/B/Li = 1:1:10:5 for $(H_3O)[(UO_2)(BO_3)]$, $UO_2(NO_3)_2\cdot(H_2O)_6$ (0.0522 g, 0.10 mmol), $Pb(NO_3)_2$ (0.0336 g, 0.10 mmol), $Li_2B_4O_7$ (0.0682 g, 0.40 mmol) and deionized water (0.5 mL) in a ratio of U/Pb/B/Li = 1:1:16:8 for $Li[(UO_2)(BO_3)]\cdot(H_2O)$,were sealed into Teflon-lined stainless steel autoclaves (23 mL). The autoclaves were heated up to 220 °C holding for 24 hours and then slowly cooled down to room temperature at a rate of 3 °C/h. The resulting products were washed with hot water and then rinsed with ethanol. Yellowish thin needle shaped crystals of $(H_3O)[(UO_2)(BO_3)]$ and $Li[(UO_2)(BO_3)]\cdot(H_2O)$ were obtained. Good quality crystals were collected for further analyses. The results of energy dispersive X-ray spectroscopy (EDS) elemental analysis and scanning electron microscopy (SEM) on several single crystals is given in Figure S1a.

4.1.2 Synthesis of α-$K_4[(UO_2)_5(BO_3)_2O_4]$: Compound α-$K_4[(UO_2)_5(BO_3)_2O_4]$ was obtained from high temperature solid state synthesis. A mixture of $UO_2(NO_3)_2\cdot(H_2O)_6$ (0.0522 g, 0.11 mmol), $K(NO_3)_2$ (0.0366 g, 0.22 mmol), $K_2B_4O_7(H_2O)_4$ (0.0628 g, 0.19 mmol) and H_3BO_3 (0.0643 g, 1.04 mmol) in a ratio of U/K/B = 1:6:18 was used. All the reactants were thoroughly ground in an agate mortar and then transferred to a platinum crucible. The reaction mixtures were heated up to 980 °C for 5 hours in a box furnace and then cooled down to 450 °C at a cooling rate of 5 °C/h. Yellow plate crystals α-$K_4[(UO_2)_5(BO_3)_2O_4]$ were obtained. Pure polycrystalline samples of α-$K_4[(UO_2)_5(BO_3)_2O_4]$were synthesized quantitatively by the reaction of a mixture of $UO_2(NO_3)_2\cdot(H_2O)_6$ (0.2028 g, 0.40 mmol), K_2CO_3 (0.0697 g, 0.50 mmol), H_3BO_3 (0.0372 g, 0.60 mmol) with a molar ratio of 4:5:4 at 900 °C for 2 days. The product obtained was characterized using X-ray powder diffraction (XRD) which indicated α-$K_4[(UO_2)_5(BO_3)_2O_4]$ that obtained material is of high purity (see Figure S2a). EDS elemental analyses on several single crystals of this compound gave an average molar ratio of U/K = 5:4.16, which is in good agreement with the results of crystallographic study (see Figure S1b).

4.1.3 Synthesis of β-$K_4[(UO_2)_5(BO_3)_2O_4]$: Compound β-$K_4[(UO_2)_5(BO_3)_2O_4]$ was synthesized via high temperature/high pressure solid state reaction. The starting chemicals of U_3O_8 (0.0536 g, 0.06 mmol), KNO_3 (0.0336 g, 0.21 mmol) and B_2O_3 (0.0698 g, 1.00 mmol) with a ratio of U/K/B = 1:3:16 for β-$K_4[(UO_2)_5(BO_3)_2O_4]$. All the reagents were thoroughly ground in an agate mortar and then transferred to a small platinum crucible. The mixtures were pressed and then sealed in the platinum crucible. A pressure of 4.0 GPa was applied within 0.5 hour and the reaction mixtures were kept 4.0 GPa for the whole experimental run. The temperature was increased up to 1000 °C in 0.5 hour, after the pressure was stable at 4.0 GPa. The temperature held at 1000 °C for 6 hours then slowly cooled down to 700 °C with a rate of 5 °C/h, cooled down to 450 °C at a rate of 10 °C/h followed by quenching to room temperature. The pressure was released in half an hour. For extracting the resulting products, the platinum crucible was crushed. The yellow pallet shaped crystals of β-$K_4[(UO_2)_5(BO_3)_2O_4]$ were isolated. EDS elemental analyses on several single crystals of β-$K_4[(UO_2)_5(BO_3)_2O_4]$ gave

Table 1. Crystallographic data for $(H_3O)[(UO_2)(BO_3)]$, $Li[(UO_2)(BO_3)]\cdot(H_2O)$, α-$K_4[(UO_2)_5(BO_3)_2O_4]$, β-$K_4[(UO_2)_5(BO_3)_2O_4]$ and $K_{2.5}[(UO_2)_5(BO_3)_2O_{2.5}(OH)_{1.5}]\cdot(H_2O)_{2.5}$.[a]

Compound	$(H_3O)[(UO_2)(BO_3)]$	$Li[(UO_2)(BO_3)]\cdot(H_2O)$	α-$K_4[(UO_2)_5(BO_3)_2O_4]$	β-$K_4[(UO_2)_5(BO_3)_2O_4]$	$K_{2.5}[(UO_2)_5(BO_3)_2O_{2.5}(OH)_{1.5}]\cdot(H_2O)_{2.5}$
FW	344.84	351.78	1688.17	1688.17	1647.99
Space group	*Pbam*	*Cmca*	$C2/_c$	*Pbam*	*Pbam*
a [Å]	11.3498(9)	6.8683(13)	15.714(3)	13.3612(3)	13.3853(5)
b [Å]	14.5959(18)	15.459(4)	11.7415(10)	11.8625(3)	23.9949(8)
c [Å]	6.8790(5)	11.231(3)	13.339(2)	6.8466(2)	6.9698(5)
α [deg]	90	90	90	90	90
β [deg]	90	90	123.690(15)	90	90
γ [deg]	90	90	90	90	90
V [Å^3]	1139.58(19)	1192.5(5)	2047.8(5)	1085.17(5)	2238.6(2)
Z	8	8	4	2	4
λ (Å)	0.71073	0.71073	0.71073	0.71073	0.71073
F(000)	1160	1184	2824	1412	2736
D_c [g cm^{-3}]	4.020	3.919	5.476	5.167	4.872
GOOF on F^2	1.125	1.131	0.862	1.164	1.067
R_1	0.0680	0.0652	0.0346	0.0382	0.0446
*wR*2	0.1708	0.1317	0.0954	0.1087	0.0951

[a] $R1 = \sum||F_o| - |F_c||/\sum|F_o|$, $wR2 = \{\sum w[(F_o)^2 - (F_c)^2]^2/\sum w[(F_o)^2]^2\}^{1/2}$.

an average molar ratio of U/K = 5:3.89, which is in good agreement with the composition obtained from crystallographic study (see Figure S1c).

4.1.4 Synthesis of $K_{2.5}[(UO_2)_5(BO_3)_2O_{2.5}(OH)_{1.5}]\cdot(H_2O)_{2.5}$: Compound $K_{2.5}[(UO_2)_5(BO_3)_2O_{2.5}(OH)_{1.5}]\cdot(H_2O)_{2.5}$was prepared through a hydrothermal method. The mixtures of $UO_2(NO_3)_2\cdot(H_2O)_6$ (0.0516 g, 0.10 mmol), $Zn(NO_3)_2(H_2O)_6$ (0.0632 g, 0.21 mmol), $K_2B_4O_7(H_2O)_4$ (0.1226 g, 0.39 mmol) and deionized water (0.5 mL), in a ratio of U/Zn/B/K = 1:2:8:16 for $K_{2.5}[(UO_2)_5(BO_3)_2O_{2.5}(OH)_{1.5}]\cdot(H_2O)_{2.5}$, was sealed into Teflon-lined stainless steel autoclaves (23 mL) and then transferred into a box furnace, heated up to 220 °C and holding for 24 hours, then slowly cooled down to room temperature with a rate of 3 °C/h. The resulting products were washed with hot water and then rinsed with ethanol. Yellow cubic block shaped crystals $K_{2.5}[(UO_2)_5(BO_3)_2O_{2.5}(OH)_{1.5}]\cdot(H_2O)_{2.5}$ were obtained. Fine crystals were collected for further analyses. EDS analysis on several single crystals gave an average molar ratio of U/K = 5:2.62, which is in good agreement with its proposed chemical compositions (see Figure S1d).

4.2. Crystallographic Studies: Single Crystal diffraction data for all five compounds were collected on an Agilent Technologies SuperNova diffractometer with Mo-K_α radiation (λ = 0.71073 Å) at room temperature. All data sets were corrected for Lorentz and polarization factors as well as for absorption by the multi-scan method.[25] The structures of all compounds were solved by direct methods and refined by a full-matrix least-squares fitting on F^2 by SHELX.[26]All structures were checked for possible missing symmetry elements using PLATON with the ADDSYM algorithm, and no higher symmetry solutions were found.[27] Crystallographic data and structural refinements for four compounds are summarized in Table 1.

X-ray powder diffraction data were collected on a Bruker-AXS D4 Endeavor diffractometer, 40 kV/40 mA, in Bragg–Brentano geometry. The diffractometer is equipped with a copper X-ray tube and a primary nickel filter producing Cu-$K_{\alpha 1,\ 2}$radiation (λ = 1.54187 Å). A linear silicon strip LynxEye detector (Bruker-AXS) was used. Data were recorded in the range of 2θ = 10–80° with 10 s/step and a step width of 0.02°. The aperture of the fixed divergence slit and the receiving slit was set to 0.2 mm and 8.0 mm, respectively. The discriminator of the detector was set to an interval from 0.16 to 0.25 V.

CCDC 1855924 {for $(H_3O)[(UO_2)(BO_3)]$}, 1855925 {for $Li[(UO_2)(BO_3)]\cdot(H_2O)$}, 1855926 {for α-$K_4[(UO_2)_5(BO_3)_2O_4]$}, 1855927 {for β-$K_4[(UO_2)_5(BO_3)_2O_4]$}, and 1855928 {for $K_{2.5}[(UO_2)_5(BO_3)_2O_{2.5}(OH)_{1.5}]\cdot(H_2O)_{2.5}$} contain the supplementary crystallographic data for this paper. These data can be obtained free of charge from The Cambridge Crystallographic Data Centre.

4.3. SEM/EDS Analysis: Scanning electron microscopy (SEM) images and EDS measurements for elemental analysis were collected on a FEI Quanta 200F Environment Scanning Electron Microscope with a low-vacuum mode at 0.6 mbar. SEM/EDS results are given as Supporting Information (Figure S1).

4.4. Thermal Analysis: The thermal behavior of the dried polycrystalline of α-$K_4[(UO_2)_5(BO_3)_2O_4]$ and $K_{2.5}[(UO_2)_5(BO_3)_2O_{2.5}(OH)_{1.5}]\cdot(H_2O)_{2.5}$ were studied by DSC analysis coupled with TG in air at temperatures of up to 1200 °C with a heating rate of 10 °C/min using a Netzsch STA 449C Jupiter apparatus. The sample (18.5 mg) was loaded in a platinum crucible, which was closed with a platinum cover. During the measurements a constant air flow of 20–30 mL/min was applied.

4.5. Raman Spectroscopy: Unpolarized Raman spectra were recorded with a Horiba LabRAM HR spectrometer using a Peltier cooled multichannel CCD detector. An objective lens with a 50 × magnification was linked to the spectrometer, allowing the analysis of samples as small as 2 μm in diameter. All the samples were in the form of single crystals. The incident radiation was produced by a He-Ne laser line at a power of 17 mW (λ = 632.8 nm). The focal length of the spectrometer was 800 mm, and an 1800 gr/mm grating was used. The spectral resolution was approximately 1 cm^{-1} with a slit of 100 μm. The spectra were recorded in the range of 100–4000 cm^{-1}.

4.6. Bond-Valence Analysis: A semi-empirical method Bond-valence sums (BVS) were applied for the determination of valence states. BVS of all atoms in the five uranyl borates phases were calculated and in a good agreement with corresponding formal values of oxidation states. The bond-valence parameters for U^{VI}–O (R_{ij}= 2.042Å and B = 0.506Å), Li^{I}–O, K^{I}–O and B^{III}–O were used according to Burns, Brese and O'Keeffe.[28–30]

Acknowledgments

E. V. A. is supported by the Deutsche Forschungsgemeinschaft (DFG) [grant DFG AL1527/3-1]. Y. H. is grateful to the Natural Science Foundation of the Education Department of Anhui

Province (KJ2019A0831) and Hefei University Talent Funding (18-19RC14). Y. H. thanks the Chinese Scholarship Council for the support. TEA-S thanks the Chemical Sciences, Geosciences, and Biosciences Division of the Office of Basic Energy Sciences of the Department of Energy for supporting this research as part of the Center for Actinide Science and Technology (CAST) funded by the U.S. Department of Energy, Office of Science, Office of Basic Energy Sciences, under Award Number DE-SC0016568. S. W. is supported by the National Natural Science Foundation of China (21761132019). Authors are grateful to Dr. Modolo, Dr. Klinkenberg, and Dr. Schlenz for their help in TG-DSC, SEM-EDS, and Raman data collection. Thanks to Dr. Kisan for revising the paper. Open access funding enabled and organized by Projekt DEAL.

Keywords: Actinides · Uranium · Borates · Structure elucidation · Topology

[1] S. Wang, E. V. Alekseev, W. Depmeier, T. E. Albrecht-Schmitt, *Chem. Commun.* **2011**, *47*, 10874–10885.
[2] M. A. Silver, T. E. Albrecht-Schmitt, *Coord. Chem. Rev.* **2016**, *323*, 36–51.
[3] A. J. Lussier, R. Lopez, P. C. Burns, *Can. Mineral.* **2017**, *54*, 177–283.
[4] P. C. Burns, *Can. Mineral.* **2005**, *43*, 1839–1894.
[5] D. L. Clark, D. E. Hobart, M. P. Neu, *Chem. Rev.* **1995**, *95*, 25–48.
[6] M. Doran, A. J. Norquist, D. O'Hare, *Chem. Commun.* **2002**, 2946–2947.
[7] G. Morrison, M. D. Smith, H.-C. zur Loye, *J. Am. Chem. Soc.* **2016**, *138*, 7121–7129.
[8] E. V. Alekseev, S. V. Krivovichev, W. Depmeier, *J. Solid State Chem.* **2009**, *182*, 2074–2080.
[9] Y. Hao, V. V. Klepov, G. L. Murphy, G. Modolo, D. Bosbach, T. E. Albrecht-Schmitt, B. J. Kennedy, S. Wang, E. V. Alekseev, *Cryst. Growth Des.* **2016**, *16*, 5923–5931.
[10] *Chemical Forms of Uranium*, Argonne National Laboratory. Retrieved 18 February, **2007**.
[11] J. J. Katz, L. R. Morss, and G. T. Seaborg, *The chemistry of the actinide elements. 2.* **1986**.
[12] L. Cheng, G. Y. Yang, *Chem. Commun.* **2014**, *50*, 344–346.
[13] Y. C. Hao, C. L. Hu, X. Xu, F. Kong, J. G. Mao, *Inorg. Chem.* **2013**, *52*, 13644–13650.
[14] Y. C. Hao, X. Xu, F. Kong, J. L. Song, J. G. Mao, *CrystEngComm* **2014**, *16*, 7689–7695.
[15] H. Behm, *Acta Crystallogr., Sect. C* **1985**, *41*, 642–645.
[16] Y. Zhang, M. Bhadbhade, J. R. Price, I. Karatchevtseva, D. Collison, G. R. Lumpkin, *RSC Adv.* **2014**, *4*, 34244–34247.
[17] S. Wang, E. V. Alekseev, J. T. Stritzinger, W. Depmeier, T. E. Albrecht-Schmitt, *Inorg. Chem.* **2010**, *49*, 6690–6696.
[18] S. Wang, E. V. Alekseev, J. T. Stritzinger, W. Depmeier, T. E. Albrecht-Schmitt, *Inorg. Chem.* **2010**, *49*, 2948–2953.
[19] S. Wang, E. V. Alekseev, J. T. Stritzinger, G. Liu, W. Depmeier, T. E. Albrecht-Schmitt, *Chem. Mater.* **2010**, *22*, 5983–5991.
[20] S. Wang, T. G. Parker, D. J. Grant, J. Diwu, E. V. Alekseev, W. Depmeier, L. Gagliardi, T. E. Albrecht-Schmitt, *Inorg. Chem.* **2012**, *51*, 11211–11213.
[21] S. Wang, E. M. Villa, J. Diwu, E. V. Alekseev, W. Depmeier, T. E. Albrecht-Schmitt, *Inorg. Chem.* **2011**, *50*, 2527–2533.
[22] S. Wu, S. Wang, M. Polinski, O. Beermann, P. Kegler, T. Malcherek, A. Holzheid, W. Depmeier, D. Bosbach, T. E. Albrecht-Schmitt, E. V. Alekseev, *Inorg. Chem.* **2013**, *52*, 5110–5118.
[23] J. T. Stritzinger, E. V. Alekseev, M. J. Polinski, J. N. Cross, T. M. Eaton, T. E. Albrecht-Schmitt, *Inorg. Chem.* **2014**, *53*, 5294–5299.
[24] K. A. Pace, V. Kocevski, S. G. Karakalos, G. Morrison, T. Besmann, H. C. zur Loye, *Inorg. Chem.* **2018**, *57*, 4244–4247.
[25] *CrystalClear*, version 1.3.5, Rigaku Corp. Woodlands, TX, **1999**.
[26] G. M. Sheldrick, *SHELXTL*, Crystallographic Software Package, version 5.1, Bruker-AXS: Madison, WI, **1998**.
[27] A. L. Spek, PLATON, Utrecht University: Utrecht, The Netherlands, **2001**.
[28] P. C. Burns, *Can. Mineral.* **1997**, *35*, 1551–1570.
[29] I. D. Brown, D. Altermatt, *Acta Crystallogr., Sect. B* **1985**, *41*, 244–247.
[30] N. E. Brese, M. O'Keeffe, *Acta Crystallogr., Sect. B* **1991**, *47*, 192–197.
[31] M. Gasperin, *Acta Crystallogr., Sect. A* **1987**, *C43*, 2031–2036.
[32] M. Gasperin, *Acta Crystallogr., Sect. A* **1987**, *C43*, 2264–2270.
[33] S. Wu, S. Wang, M. J. Polinski, W. Depmeier, T. E. Albrecht-Schmitt, E. V. Alekseev, *Z. Kristallogr.* **2013**, *228*, 429–434.
[34] D. K. Smith, J. W. Gruner, W. N. Lipscomb, *Am. Mineral.* **1957**, *b42*, 594–599.
[35] P. C. Burns, M. L. Miller, R. C. Ewing, *Can. Mineral.* **1996**, *34*, 845–880.
[36] P. C. Burns, J. D. Grice, F. C. Hawthorne, *Can. Mineral.* **1995**, *33*, 1131–1151.
[37] E. V. Alexandrov, V. A. Blatov, A. V. Kochetkov, *CrystEngComm* **2011**, *13*, 3947–3958.
[38] V. A. Blatov, M. O'Keeffe, D. M. Proserpio, *CrystEngComm* **2010**, *12*, 667–675.
[39] V. A. Blatov, *IUCr CompComm Newsletter* **2006**, *7*, 4–38.
[40] P. Piret, M. Deliens, J. Piretmeunier, G. Germain, *Bull. Mineral.* **1983**, *106*, 299–304.
[41] M. Gasperin, *Acta Crystallogr., Sect. A* **1989**, *45*, 981–988.
[42] S. Wang, E. V. Alekseev, J. Ling, G. Liu, W. Depmeier, T. E. Albrecht-Schmitt, *Chem. Mater.* **2010**, *22*, 2155–2163.
[43] X. Xu, Z. Liu, S. Yang, L. Chen, J. Diwu, E. V. Alekseev, Z. Chai, T. E. Albrecht-Schmitt, S. Wang, *Dalton Trans.* **2016**, *45*, 15464–15472.
[44] Y. Hao, P. Kegler, D. Bosbach, T. E. Albrecht-Schmitt, S. Wang, E. V. Alekseev, *Cryst. Growth Des.* **2017**, *17*, 5898–5907.
[45] K. Nakamoto, A. Part, *Infrared and Raman Spectra of Inorganic and Coordination Compounds* John Wiley & Sons, Inc. **2009**.
[46] Y. Hao, L. He, G. Ge, Q. Zhang, N. Luo, S. Huang, H. Li, V. Alekseev, *J. Solid State Chem.* **2020**, *281*, 121046–121052.
[47] G. Barros, E. N. Silva, A. P. Ayala, I. Guedes, C.-K. Loong, J. Y. Wang, *Vib. Spectrosc.* **2008**, *46*, 100–106.
[48] Y. Hao, G. L. Murphy, D. Bosbach, G. Modolo, T. E. Albrecht-Schmitt, E. V. Alekseev, *Inorg. Chem.* **2017**, *56*, 9311–9320.

Received: November 18, 2019